Matrix Isolation FTIR Spectroscopic and Density Functional Theoretical Studies of the Reactions of Magnesium Atoms with Methanol

Zhengguo Huang, Mohua Chen, Qingnan Liu, and Mingfei Zhou*

Shanghai Key Laboratory of Molecular Catalysts and Innovative Materials, Department of Chemistry, Fudan University, Shanghai 200433, P.R. China

Received: June 11, 2003; In Final Form: October 22, 2003

The reactions of magnesium atoms and methanol molecules have been investigated with matrix-isolation FTIR spectroscopy. In solid argon, the ground-state Mg atom reacted with methanol to form the Mg(CH_3-OH) complex spontaneously on annealing. The complex underwent photochemical rearrangement to the methylmagnesium hydroxide (CH_3MgOH) molecule upon ultraviolet−visible irradiation. The CH_3MgOH molecule further reacted with a magnesium atom to form the $CH_3MgOMgH$ molecule. The aforementioned species were identified on the basis of isotopic IR studies with $^{13}CH_3OH$, $CH_3{}^{18}OH$, and CH_3OD, as well as density functional theory calculations.

Introduction

The conversion of methane to methanol has been widely studied due to its great economic and scientific importance.[1] The prototypical reaction $MO + CH_4 \rightarrow CH_3OH + M$ and its reverse reaction have gained much attention in providing fundamental information regarding the catalytic conversion process of CH_4 to CH_3OH. The reactivity of transition metal monoxide cations (MO^+) toward methane has been systematically investigated experimentally.[2,3] The results showed that the reaction efficiency and the methanol branching ratio depend significantly on the metals. The reaction has been proposed to proceed via an insertion intermediate (CH_3-M^+-OH). Theoretical studies indicated that the reaction pathway from methane to methanol is uphill in energy on the early MO^+ cations, whereas the late MO^+ cations are expected to efficiently convert methane to methanol.[4]

The reactions of metal atoms with methanol also have gained considerable attention. Matrix isolation spectroscopy provides a powerful method to investigate thermal and photochemical reactions between atoms and small molecules.[5−9] An earlier study of the iron atom reaction with methanol has identified the formation of the Fe(CH_3OH) complex. Subsequent photoexcitation of the complex in the visible region ($\lambda > 400$ nm) led to iron insertion into the O−H bond, whereas UV (280 nm $< \lambda <$ 360 nm) irradiation caused the activation of the C−O bond.[10] Silicon atoms inserted into both the O−H and C−O bonds of methanol to form methoxysilylene and methylsilicon hydroxide in solid argon, but the O−H bond insertion is energetically favored over the C−O bond insertion.[11,12] The reactions of laser-ablated boron atoms with methanol produced CH_3BO as well as CH_2BOH and CH_2BO.[13] All of these products were formed via boron insertion into the C−O bond. In contrast, no electron paramagnetic resonance evidence was found for aluminum atom insertion into the C−O, C−H, and O−H bonds of methanol in an adamantine matrix at 77K.[14] Apparently, the reactivity of methanol toward metal atoms is diverse and heavily depends on the metals.

In this paper, we report a combined matrix isolation FTIR spectroscopic and theoretical investigation on the reactions of magnesium atoms with methanol. MgO has been found to be one of the most effective catalysts for methane to methanol conversion.[15] Recently, the reaction of $CH_4 + MgO \rightarrow Mg + CH_3OH$ has been theoretically studied at the MP2 level.[16] To our knowledge, no experimental study has been reported on the reactions between CH_4 and MgO or CH_3OH and Mg. Previous matrix isolation infrared studies of the alkaline earth metal atom interactions with water in solid argon revealed that magnesium atoms inserted into the O−H bonds of water to form HMgOH and HMgOMgH.[17] The methanol reactions resemble the water reactions, but with one hydrogen atom replaced by a methyl group. Therefore, metal atom insertion into CH_3OH can take place in a C−O, O−H, or C−H bond.

Experimental and Theoretical Methods

The experimental setup for pulsed laser ablation and matrix infrared spectroscopic investigation has been described previously.[18] Briefly, the 1064-nm Nd:YAG laser fundamental (Spectra Physics, DCR 150, 20 Hz repetition rate and 8 ns pulse width) was focused onto the rotating magnesium metal target, and the ablated metal atoms were co-deposited with methanol in excess argon onto a 12 K CsI window, which was mounted on a cold tip of a closed-cycle helium refrigerator (Air Products, Model CSW202) for 1 h at a rate of approximately 2−4 mmol/h. Typically, 5−10 mJ/pulse laser power was used. Methanol was subjected to several freeze−pump−thaw cycles to minimize possible atmospheric contamination. The isotopic CH_3OD (Merck, 99%), $^{13}CH_3OH$ and $CH_3{}^{18}OH$ (99%, Cambridge Isotopic Laboratories), and selected mixtures were used in different experiments. Infrared spectra were recorded on a Bruker IFS113V spectrometer at 0.5 cm^{-1} resolution, using a DTGS detector. Matrix samples were annealed at different temperatures, and selected samples were subjected to broadband irradiation with use of a 250-W high-pressure mercury arc lamp with the globe removed.

Density functional calculations were performed with the Gaussian 98 program.[19] The three-parameter hybrid functional according to Becke with additional correlation corrections due to Lee, Yang, and Parr was utilized (B3LYP).[20,21] The 6-311++G** basis sets were used.[22,23] The geometries were

* Corresponding author. E-mail: mfzhou@fudan.edu.cn.

10.1021/jp035652z CCC: $25.00
Published on Web 11/26/2003

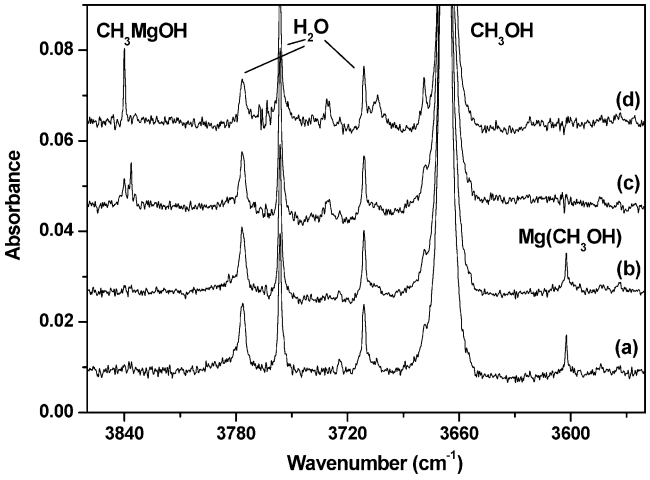

Figure 1. Infrared spectra in the 3860−3560-cm^{-1} region from co-deposition of laser-ablated magnesium atoms and 0.2% CH_3OH in argon: (a) 1-h sample deposition at 12 K, (b) after 25 K annealing, (c) after 30 min broadband photolysis, and (d) after 30 K annealing.

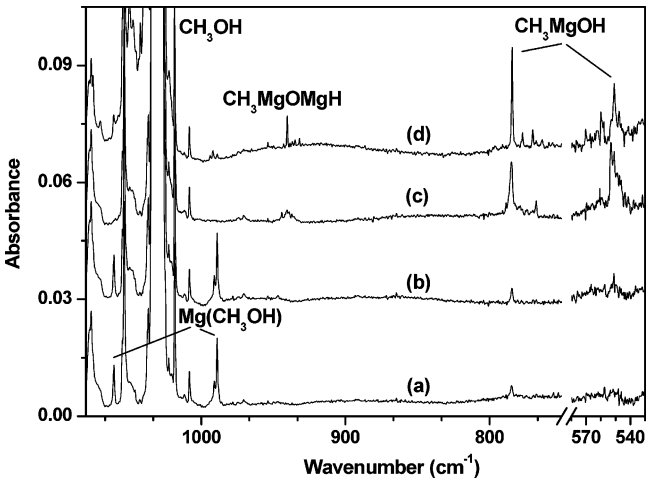

Figure 2. Infrared spectra in the 1080−750- and 580−530-cm^{-1} regions from co-deposition of laser-ablated magnesium atoms and 0.2% CH_3OH in argon: (a) 1-h sample deposition at 12 K, (b) after 25 K annealing, (c) after 30 min broadband photolysis, and (d) after 30 K annealing.

fully optimized; the harmonic vibrational frequencies were calculated with analytic second derivatives, and zero-point vibrational energies (ZPVE) were derived. Transition state optimizations were done with the synchronous transit-guided quasi-Newton (STQN) method[24] at the B3LYP/6-311++G** level followed by the vibrational frequency calculations showing the obtained structures to be true saddle points.

Results and Discussions

The IR spectra of the reaction products with various isotopic combinations are reported, and the product absorptions will be assigned by consideration of the frequencies and isotopic shifts of the observed bands and by comparisons with DFT frequency calculations.

Infrared Spectra. The infrared spectra in selected regions from co-deposition of laser-ablated Mg atoms with methanol molecules in excess argon are illustrated in Figures 1 and 2, respectively, and the product absorptions are listed in Table 1. The stepwise annealing and irradiation behavior of the product absorptions is also shown in the figures and will be discussed below. Carbon-13, oxygen-18, and deuterium substitution experiments were employed for product identification through isotopic shift and splitting, and the isotopic counterparts are also listed in Table 1. Representative spectra in selected regions with different isotopic samples are shown in Figures 3−6, respectively.

Calculation Results. The most popular DFT/B3LYP calculations which can provide very reliable predictions of the state energies, structures, and vibrational frequencies were performed on the potential reaction products.[25] Three $MgCH_3OH$ isomers, namely, the $Mg(CH_3OH)$ complex, the inserted methylmagnesium hydroxide (CH_3MgOH) and methoxylmagnesium hydride (CH_3OMgH) molecules, were considered. The optimized geometric parameters are shown in Figure 7, and the vibrational frequencies and intensities are listed in Table 2. All three structural isomers were predicted to have a singlet ground state and to be stable with respect to the ground-state reactants: Mg + CH_3OH. Both the inserted CH_3MgOH and CH_3OMgH molecules were predicted to have C_{3v} symmetry and the $Mg(CH_3OH)$ complex was predicted to have C_s symmetry. The ground-state ($^1A_1$) CH_3MgOH molecule is the global minimum at this level of theory. The CH_3OMgH ($^1A_1$) molecule is 19.5 kcal/mol higher in energy than CH_3MgOH, and the $Mg(CH_3OH)$ ($^1A'$) complex is about 39.0 kcal/mol less stable than CH_3MgOH. The geometries and vibrational frequencies of $Mg(CH_3OH)$ and CH_3MgOH were recently addressed by Hu and co-workers using the MP2 method.[16] These calculations predicted the $Mg(CH_3OH)$ complex to have C_1 symmetry, in disagreement with our B3LYP calculations. However, we note that the calculated geometries at the B3LYP and MP2 levels are quite similar, the major difference being the relative positions of the H atoms in the CH_3 subunit. The MP2 results on CH_3MgOH are in good agreement with our B3LYP calculations.

Similar calculations were also done on the $CH_3MgOMgH$ molecule. The optimized structure is also shown in Figure 7 and the vibrational frequencies and intensities are listed in Table 2.

$Mg(CH_3OH)$. The absorptions at 989.0, 1060.4, 1439.9, and 3602.4 cm^{-1} are assigned to the $Mg(CH_3OH)$ molecule. These absorptions were observed after sample deposition, increased together on annealing in low CH_3OH concentration experiments, and disappeared on UV−visible irradiation. The 3602.4-cm^{-1} band showed no carbon-13 isotopic shift, but shifted to 3591.2 cm^{-1} with $CH_3{}^{18}OH$ and to 2662.6 cm^{-1} with CH_3OD. The band position and isotopic H/D ratio of 1.3530 and $^{16}O/^{18}O$ ratio of 1.0031 indicate that the 3602.4-cm^{-1} band is due to an O−H stretching vibration. In the mixed $CH_3{}^{16}OH$ + $CH_3{}^{18}OH$ experiment, only the pure isotopic counterparts were observed, indicating that only one OH subunit is involved in this molecule. The 989.0-cm^{-1} band shifted to 963.5 cm^{-1} with $CH_3{}^{18}OH$, and to 970.5 cm^{-1} with $^{13}CH_3OH$. The isotopic $^{16}O/^{18}O$ ratio of 1.0265 and $^{12}C/^{13}C$ ratio of 1.0191 suggest a C−O stretching vibration. The 1060.4-cm^{-1} band exhibited no isotopic shift with $CH_3{}^{18}OH$, but shifted to 857.7 cm^{-1} with CH_3OD, and to 1057.2 cm^{-1} with $^{13}CH_3OH$. This band is assigned to the CH_3OH deformation mode. As shown in Figure 3, the 989.0-cm^{-1} band split into doublets in the experiments with mixed $CH_3{}^{16}OH$ + $CH_3{}^{18}OH$ and $^{12}CH_3OH$ + $^{13}CH_3OH$ samples, while the 1060.4-cm^{-1} band split into doublets in the $^{12}CH_3OH$ + $^{13}CH_3OH$ and CH_3OH + CH_3OD experiments, indicating that the molecule contains only one CH_3OH unit. The 1439.9-cm^{-1} band showed very small isotopic shift with $CH_3{}^{18}OH$, CH_3OD, and $^{13}CH_3OH$, and is assigned to the CH_3 deformation mode of the $Mg(CH_3OH)$ complex.

The assignment is supported by the DFT calculations. The four experimentally observed vibrational modes of $Mg(CH_3$-

TABLE 1: Infrared Absorptions (cm^{-1}) from Co-deposition of Laser-Ablated Magnesium Atoms with Methanol in Excess Argon

$CH_3{}^{16}OH$	$CH_3{}^{18}OH$	$^{13}CH_3OH$	CH_3OD	assignment
551.0	549.3	547.6	550.5	CH_3MgOH, $\delta(CH_3)$
784.4	768.5	782.5	774.2	$CH_3{}^{24}MgOH$, ν(Mg−OH)
777.2	761.2	775.9	765.9	$CH_3{}^{25}MgOH$, ν(Mg−OH)
770.1	753.8	768.9	758.4	$CH_3{}^{26}MgOH$, ν(Mg−OH)
3840.1	3827.9	3840.1		CH_3MgOH, ν(O−H)
940.4	902.8	940.3	935.2	$CH_3{}^{24}MgO^{24}MgH$, ν(Mg−O−Mg)
938.5	900.9	938.5		$CH_3{}^{24}MgO^{25}MgH$, ν(Mg−O−Mg)
936.8	899.3	936.5		$CH_3{}^{25}MgO^{24}MgH$, ν(Mg−O−Mg)
935.0	897.5	934.7		$CH_3{}^{24}MgO^{26}MgH$, ν(Mg−O−Mg)
932.0	896.6	932.0		$CH_3{}^{26}MgO^{24}MgH$, ν(Mg−O−Mg)
1541.4	1541.3	1541.3	1125.0	$CH_3MgOMgH$, ν(Mg−H)
989.0	963.5	970.5	989.0	$Mg(CH_3OH)$, ν(C−O)
1060.4	1060.3	1057.2	857.7	$Mg(CH_3OH)$, $\delta(CH_3OH)$
1439.9	1439.3	1434.5	1439.8	$Mg(CH_3OH)$, $\delta(CH_3)$
3602.4	3591.2	3602.4	2662.6	$Mg(CH_3OH)$, ν(O−H)

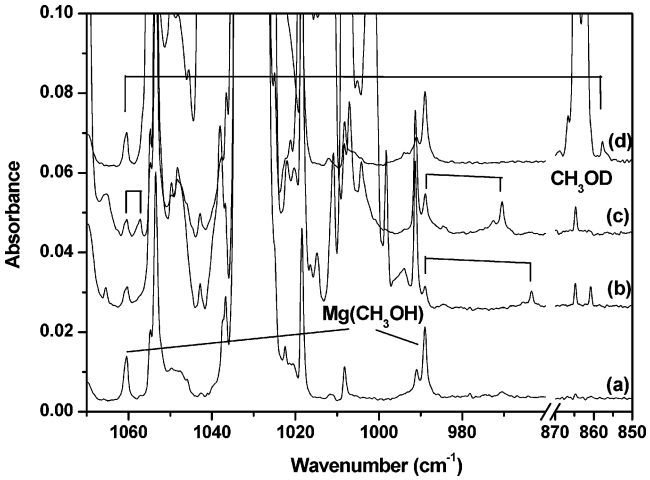

Figure 3. Infrared spectra in the 1070−960- and 870−850-cm^{-1} regions from co-deposition of laser-ablated magnesium atoms with different isotopic samples in excess argon and annealed to 25 K: (a) 0.2% CH_3OH, (b) 0.1% $CH_3{}^{16}OH$ + 0.1% $CH_3{}^{18}OH$, (c) 0.1% $^{12}CH_3OH$ + 0.1% $^{13}CH_3OH$, and (d) 0.1% CH_3OH + 0.1% CH_3OD.

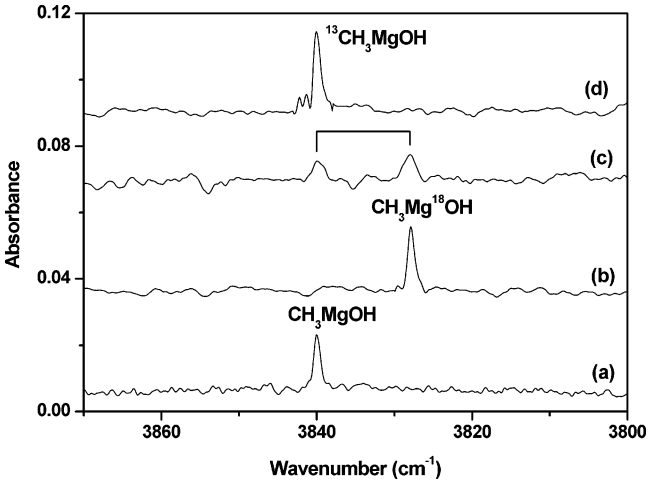

Figure 4. Infrared spectra in the 3870−3800-cm^{-1} region from co-deposition of laser-ablated magnesium atoms with different isotopic samples in excess argon: (a) 0.2% CH_3OH, (b) 0.2% $CH_3{}^{18}OH$, (c) 0.1% $CH_3{}^{16}OH$ + 0.1% $CH_3{}^{18}OH$, and (d) 0.2% $^{13}CH_3OH$. Spectra were recorded after 30 min of photolysis.

OH) were calculated at 993.9, 1062.6, 1465.2, and 3770.5 cm^{-1}, respectively, which are in excellent agreement with the observed argon matrix values. As listed in Table 3, the calculated isotopic frequency ratios also fit the experimental values very well.

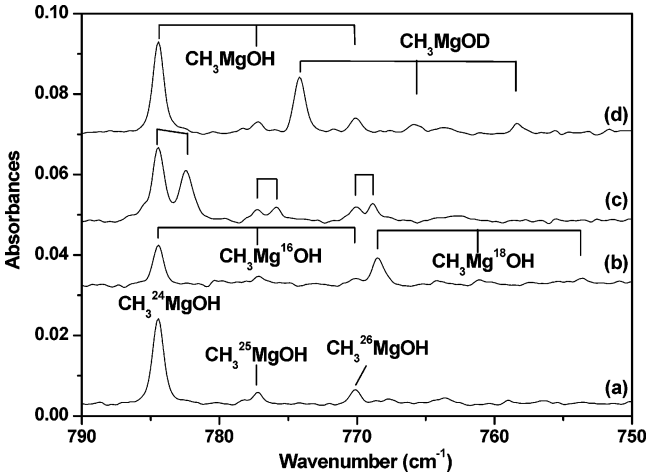

Figure 5. Infrared spectra in the 790−750-cm^{-1} region from co-deposition of laser-ablated magnesium atoms with different isotopic samples in excess argon: (a) 0.2% CH_3OH, (b) 0.1% $CH_3{}^{16}OH$ + 0.1% $CH_3{}^{18}OH$, (c) 0.1% $^{12}CH_3OH$ + 0.1% $^{13}CH_3OH$, and (d) 0.1% CH_3OH + 0.1% CH_3OD. Spectra were recorded after 30 min of photolysis and annealing to 30 K.

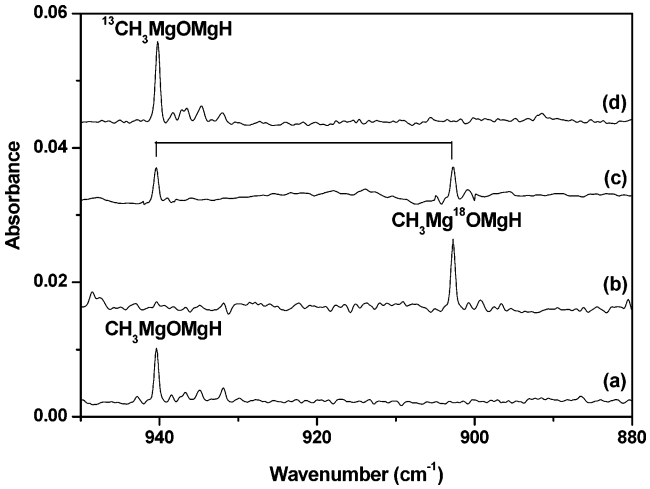

Figure 6. Infrared spectra in the 950−880-cm^{-1} region from co-deposition of laser-ablated magnesium atoms with different isotopic samples in excess argon: (a) 0.2% CH_3OH, (b) 0.2% $CH_3{}^{18}OH$, (c) 0.1% $CH_3{}^{16}OH$ + 0.1% $CH_3{}^{18}OH$, and (d) 0.2% $^{13}CH_3OH$. Spectra were recorded after 30 min of photolysis.

Besides the above characterized vibrational modes, the asymmetric and symmetric C−H stretching modes were predicted to have appreciable intensities (Table 2); however, we were not

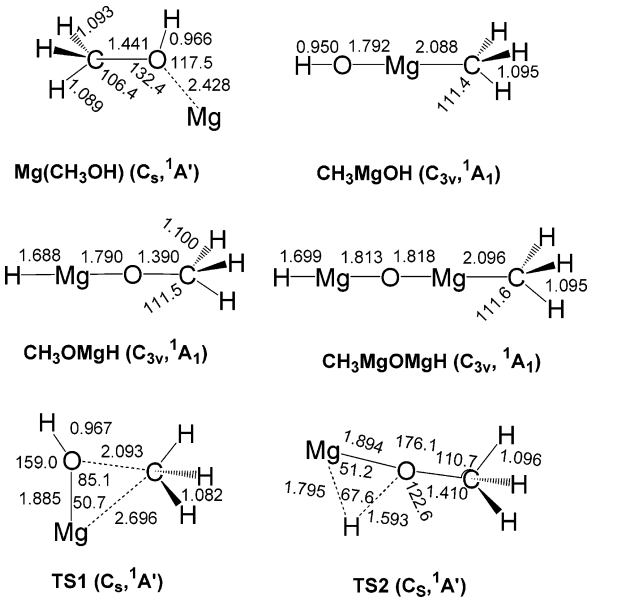

Figure 7. Optimized structures (bond lengths in Å, bond angles in degree) of the three Mg(CH_3OH) isomers, the $CH_3MgOMgH$ molecules, and the transition states on the potential energy surfaces.

TABLE 2: Calculated (B3LYP/6-311++G) Vibrational Frequencies (cm^{-1}) and Intensities (Values in Parentheses in km/mol) of the Reaction Products Shown in Figure 7**

Mg(CH_3OH)	59.0 (8.2), 89.1 (4.3), 126.1 (11.8), 292.8 (64.2), 993.9 (80.0), 1062.6 (36.4), 1157.9 (0.9), 1343.7 (19.2), 1465.2 (5.7), 1494.0 (2.0), 1505.2 (9.0), 3027.4 (50.1), 3093.1 (24.3), 3130.4 (10.5), 3770.5 (65.0)
CH_3MgOH	122.2 (99.7× 2), 186.3 (97.1 × 2), 477.3 (0.0), 602.5 (79.1 × 2), 793.4 (147.3), 1165.9 (0.4), 1455.9 (0.0 × 2), 3007.1 (27.0), 3079.3 (16.8 × 2), 4056.3 (89.7)
CH_3OMgH	116.4 (9.3× 2), 336.0 (292.7 × 2), 592.1 (19.6), 1181.4 (0.1 × 2), 1230.4 (351.3), 1485.5 (21.7), 1498.3 (0.9 × 2), 1660.9 (168.5), 2947.4 (165.2), 2987.6 (83.9 × 2)
$CH_3MgOMgH$	62.8 (1.7× 2), 160.7 (24.9 × 2), 354.5 (305.9 × 2), 371.1 (0.9), 588.0 (88.0 × 2), 600.3 (7.4), 941.4 (310.5), 1162.6 (0.3), 1455.2 (0.0 × 2), 1630.2 (235.9), 3004.7 (36.8), 3074.9 (20.3 × 2)

able to observe these bands. As has been pointed out,[26,27] DFT calculations do not provide very reliable IR intensity predictions in some cases. It is found that the IR intensities of the vibrations such as C−H stretching are substantially overestimated by DFT calculations.[28, 29]

The ground state of Mg(CH_3OH) reflects the Mg $2s^2$ ground electron configuration. Compared to free methanol, the geometry of the CH_3OH unit in the complex does not have a significant change. The small deformation of the CH_3OH ligand and the rather long Mg−O distance (2.428 Å) indicate a weak interaction between Mg and CH_3OH. The binding energy of Mg(CH_3OH) with respect to Mg + CH_3OH was predicted to be only 1.1 kcal/mol at the B3LYP/6-311++G** level after zero-point vibrational energy (ZPVE) and basis set superposition error (BSSE) corrections. This value is slightly lower than that calculated at the MP2/6-311+G(2d,2p) level.[16]

Taking the C−O stretching mode as an example, the interaction of Mg with CH_3OH causes the frequency to red-shift by about 44.7 cm^{-1}, in good agreement with the DFT calculated value of 47.3 cm^{-1}. As expected, this shift is smaller than that of the Si(CH_3OH) and Fe(CH_3OH) complexes (68.7 and 61.5 cm^{-1}, respectively).[10−12]

CH_3MgOH. Absorptions at 3840.1, 784.4, 777.2, 770.1, and 551.0 cm^{-1} are very weak after sample deposition, but markedly increased on broadband irradiation. These bands maintained the same relative intensities throughout all the experiments, suggesting that they are due to different vibrational modes of the same species, and are assigned to the CH_3MgOH molecule. The 3840.1-cm^{-1} band lies in the region expected for an O−H stretching vibration. This band showed no carbon-13 isotopic shift with $^{13}CH_3OH$, but shifted to 3827.9 cm^{-1} with $CH_3{}^{18}OH$. The isotopic $^{16}O/^{18}O$ ratio of 1.0032 is indicative of the O−H stretching vibration. In the mixed $CH_3{}^{16}OH$ + $CH_3{}^{18}OH$ experiment (Figure 4c), only the pure isotopic counterparts were observed, indicating that only one OH subunit is involved in this mode. The CH_3OD counterpart probably was overlapped by the strong CH_3OD absorptions. The relative intensities of the 784.4-, 777.2-, and 770.1-cm^{-1} bands matched the natural isotopic abundance of ^{24}Mg, ^{25}Mg, and ^{26}Mg, which clearly indicates one Mg atom involvement.[30] These three bands showed small shifts with $^{13}CH_3OH$, and shifted to 768.5, 761.2, and 753.8 cm^{-1} with $CH_3{}^{18}OH$ and to 774.2, 765.9, and 758.4 cm^{-1} with CH_3OD. The isotopic shifts indicate a Mg−OH stretching vibration. The 551.0-cm^{-1} band is due to a CH_3 deformation mode. This band exhibited very small shifts with $^{13}CH_3OH$ (3.4 cm^{-1}), $CH_3{}^{18}OH$ (1.7 cm^{-1}), and CH_3OD (0.5 cm^{-1}).

The calculated frequencies at the optimized geometry of CH_3MgOH provide excellent support for the proposed identification of this molecule. The O−H and Mg−OH stretching and the CH_3 deformation modes were computed at 4056.3, 793.4, and 602.5 cm^{-1}, respectively, which require scaling factors (observed frequency/calculated frequency) of 0.947, 0.989, and 0.915 to fit the observed values. All three modes were calculated to be intense. As listed in Table 3, the overall agreement between the calculated and observed isotopic frequency ratios is also quite convincing.

$CH_3MgOMgH$. A broad band centered at 940 cm^{-1} appeared on broadband irradiation. The band was sharpened on 30 K annealing and resolved as a quintet at 940.4, 938.5, 936.8, 935.0, and 932.0 cm^{-1} with approximately 8:1:1:1:1 relative intensities. This suggests that two inequivalent magnesium atoms are involved in this mode. Statistically, a vibration involving two inequivalent magnesium atoms should split into nine absorptions with approximately 64:8:8:8:8:1:1:1:1 relative intensities, using natural abundance magnesium (^{24}Mg, 79.0%; ^{25}Mg, 10.0%; ^{26}Mg, 11.0%). The observed quintet corresponds to the vibrations involving at least one ^{24}Mg. The other four components with the lowest intensities are too weak to be observed in our experiments. These absorptions exhibited very small shifts with $^{13}CH_3OH$ and CH_3OD, but large shifts with $CH_3{}^{18}OH$ (Table 1). In the mixed $CH_3{}^{16}OH$ + $CH_3{}^{18}OH$ experiments, only the pure isotopic counterparts were observed, indicating that only one O atom is involved in this mode. The isotopic $^{16}O/^{18}O$ ratio of 1.0416 (940.4-cm^{-1} band) is substantially higher than that of diatomic MgO,[31] suggesting a Mg−O−Mg stretching vibration. These bands are associated with a 1541.4-cm^{-1} band, which underwent a large deuterium shift, but no apparent oxygen and carbon shifts, and is due to a Mg−H stretching vibration. In the previous Mg + H_2O experiments,[17] similar bands at 936.7 and 1561.3 cm^{-1} have been assigned to the HMgOMgH molecule. Accordingly we assign the 940.4- and 1541.4-cm^{-1} bands to the $CH_3MgOMgH$ molecule.

Our DFT/B3LYP calculations predicted that the $CH_3MgOMgH$ molecule has a $^1A_1$ ground state with C_{3v} symmetry (Figure 7). The Mg−H and Mg−O−Mg stretching vibrational frequencies were computed at 1630.2 and 941.4 cm^{-1} with the

TABLE 3: Comparison of the Observed and Calculated Isotopic Frequency Ratios of the Reaction Products

		$^{16}O/^{18}O$		$^{12}C/^{13}C$		H/D	
molecule	mode	obsd	calcd	obsd	calcd	obsd	calcd
$Mg(CH_3OH)$	ν(CO)	1.0265	1.0268	1.0191	1.0197	1.0000	1.0026
	$\delta(CH_3OH)$	1.0001	1.0000	1.0030	1.0027	1.2363	1.2386
	$\delta(CH_3)$	1.0004	1.0003	1.0038	1.0041	1.0001	1.0011
	ν(OH)	1.0031	1.0033	1.0000	1.0000	1.3530	1.3732
CH_3MgOH	$\delta(CH_3)$	1.0031	1.0000	1.0062	1.0060	1.0009	1.0005
	ν(MgOH)	1.0207	1.0227	1.0024	1.0014	1.0132	1.0137
	ν(OH)	1.0032	1.0035	1.0000	1.0000		1.3708
$CH_3MgOMgH$	ν(MgOMg)	1.0416	1.0424	1.0001	1.0001	1.0056	1.0057
	ν(MgH)	1.0001	1.0000	1.0001	1.0000	1.3701	1.3779

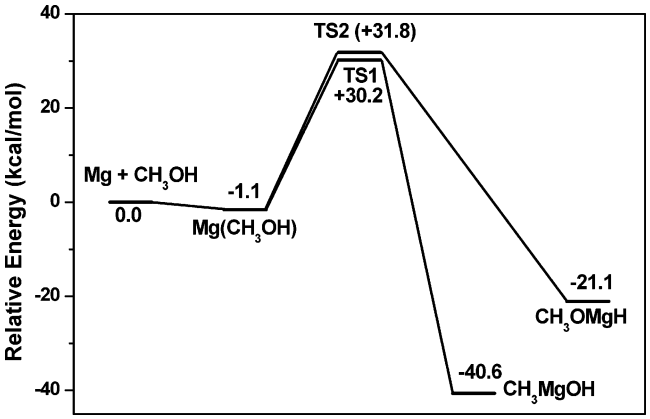

Figure 8. Potential energy profiles for the reaction of Mg + CH_3OH (relative energies are given in kcal/mol).

isotopic shifts also in good agreement with the experimental values (Table 3).

Reaction Mechanisms. Co-condensation of laser-ablated Mg atoms and methanol molecules in excess argon resulted in reaction 1 forming the $Mg(CH_3OH)$ complex as the primary reaction product. The complex absorptions increased upon annealing in low CH_3OH concentration experiments, indicating that reaction 1 requires no activation energy.

$$Mg\ (^1S) + CH_3OH\ (^1A') \rightarrow Mg(CH_3OH)\ (^1A') \qquad (1)$$

$$\Delta E = -1.1\ \text{kcal/mol}$$

The absorptions due to $Mg(CH_3OH)$ decreased on $\lambda > 290$ nm irradiation, during which the absorptions of CH_3MgOH markedly increased. It appears that the $Mg(CH_3OH)$ complex underwent photoinduced isomerism to CH_3MgOH, as shown in reaction 2.

$$Mg(CH_3OH) + \lambda > 290\ \text{nm} \rightarrow CH_3MgOH \qquad (2)$$

Similar insertion reactions have been observed in previous studies of methanol reaction with metal atoms.[10−13] Atom insertion into CH_3OH can take place in a C−H, C−O, or O−H bond. Both the C−O and O−H bond insertion reactions have been observed.[10−13] In the Mg + CH_3OH reaction, there is no experimental evidence for the O−H bond insertion. The potential energy profiles of the Mg + CH_3OH reactions composed on the basis of DFT/B3LYP calculated relative energies of the products and transition states are shown in Figure 8. The initial step of the Mg + CH_3OH reaction is the formation of the $Mg(CH_3OH)$ complex, which proceeds without any energy barrier. The further insertions of Mg atoms into either the C−O or the O−H bond of methanol were predicted to proceed via two different transition states (TS1 and TS2). The optimized transition state structures are shown in Figure 7. TS1 is the transition state for the C−O bond insertion reaction. It was predicted to have a $^1A'$ ground state with C_s symmetry. The calculated structural parameters and frequencies are consistent with that reported by Hu and co-workers at the MP2/6-311+G(2d,2p) level.[16] This transition state lies 30.2 kcal/mol higher in energy than the ground-state reactants: Mg (^1S) + CH_3OH ($^1A'$). Therefore, the energy barrier for the reaction from $Mg(CH_3OH)$ to CH_3MgOH was estimated to be 31.8 kcal/mol.

The transition state TS2 connects the $Mg(CH_3OH)$ and CH_3OMgH molecules. It was predicted to have C_s symmetry. The Mg−O and Mg−H distances are longer than those in CH_3OMgH. The O−H bond has been significantly weakened compared to that in $Mg(CH_3OH)$. This transition state was predicted to be 31.8 kcal/mol higher in energy than the separated reactants, Mg (^1S) + CH_3OH ($^1A'$), and the energy barrier for the $Mg(CH_3OH) \rightarrow CH_3OMgH$ reaction was estimated to be 32.9 kcal/mol.

The energy profiles shown in Figure 8 indicate that both the C−O and O−H bond insertion reactions require activation energy. The formation of CH_3MgOH is a photochemical process, and most likely involves an excited-state species. It is unclear that the O−H bond insertion reaction product is not observed in the experiments; we note that the CH_3OMgH molecule was predicted to be about 19.5 kcal/mol higher in energy than the CH_3MgOH isomer.

According to recent theoretical studies,[16] the CH_3MgOH molecule could further rearrange to the $OMgCH_4$ complex, and then to CH_4 + MgO. This process was predicted to be endothermic and to proceed via a transition state lying 80.9 kcal/mol higher in energy than CH_3MgOH. No evidence was found for the formation of the MgO and CH_4 molecules or the $OMgCH_4$ complex in the experiments. However, the $CH_3MgOMgH$ molecule was produced upon broadband irradiation, during which the CH_3MgOH absorptions slightly decreased. This suggests that $CH_3MgOMgH$ was formed from reaction 3 of one additional Mg atom insertion into the O−H bond of CH_3MgOH.

$$CH_3MgOH + Mg + \lambda > 250\ \text{nm} \rightarrow CH_3MgOMgH \qquad (3)$$

The magnesium and methanol reactions were found to track closely the magnesium and water reactions, with one hydrogen atom replaced by a methyl group. Analogously, the magnesium atom reacted with water to form the $Mg(H_2O)$ complex. Subsequent irradiation resulted in the insertion reactions to form the HMgOH and HMgOMgH molecules.[17]

Conclusions

The reactions of Mg atoms with methanol molecules have been investigated with matrix isolation FTIR spectroscopy and density functional theoretical calculations. The magnesium atoms were produced by laser ablation. In solid argon matrix,

magnesium atoms reacted with methanol to form the $Mg(CH_3OH)$ complex. This complex is weakly bound. The binding energy with respect to the dissociation limit $Mg + CH_3OH$ was predicted to be only 1.1 kcal/mol after ZPVE and BSSE corrections. Subsequent broadband irradiation of the $Mg(CH_3OH)$ complex resulted in the insertion reaction forming the CH_3MgOH molecule. This isomerization reaction was predicted to be exothermic and proceeded via a transition state. The CH_3MgOH molecule further reacted with the magnesium atom to form $CH_3MgOMgH$. The aforementioned species were identified via isotopic substitutions as well as density functional calculations.

Acknowledgment. The authors acknowledge financial support from NSFC (20003003 and 20125033) and the NKBRSF of China.

References and Notes

(1) Gesser, H. D.; Hunter, N. R.; Prakash, C. B. *Chem. Rev.* **1988**, *85*, 235.

(2) Schroder, D.; Schwarz, H. *Angew. Chem., Int. Ed*. **1990**, 29, 1433. Schroder, D.; Fiedler, A.; Hrusak, J.; Schwarz, H. *J. Am. Chem. Soc*. **1992**, *114*, 1215. Ryan, M. F.; Fiedler, A.; Schroder, D.; Schwarz, H. *J. Am. Chem. Soc*. **1995**, *117*, 2033. Ryan, M. F.; Fiedler, A.; Schroder, D.; Schwarz, H. *Organometallics* **1994**, *13*, 4072. Schroder, D.; Schwarz, H. *Angew. Chem., Int. Ed*. **1995**, *34*, 1973.

(3) Clemmer, D. E.; Aristov, N.; Armentrout, P. B. *J. Phys. Chem*. **1993**, *97*, 544. Chen, Y. M.; Clemmer, D. E.; Armentrout, P. B. *J. Am. Chem. Soc*. **1994**, *116*, 7815.

(4) Shiota, Y.; Yoshizawa, K. *J. Am. Chem. Soc*. **2000**, *122*, 12317 and references therein.

(5) Himmel, H. J.; Downs, A. J.; Greene, T. M. *Chem. Rev*. **2002**, *102*, 4191.

(6) Bondybey, V. E.; Smith, A. M.; Agreiter, J. *Chem. Rev*. **1996**, *96*, 2113.

(7) Zhou, M. F.; Zhang, L. N.; Dong, J.; Qin, Q. Z. *J. Am. Chem. Soc*. **2000**, *122*, 10680. Zhang, L. N.; Dong, J.; Zhou, M. F. *J. Phys. Chem. A* **2000**, *104*, 8882. Zhang, L. N.; Zhou, M. F.; Shao, L. M.; Wang, W. N.; Fan, K. N.; Qin, Q. Z. *J. Phys. Chem. A* **2001**, *105*, 6998.

(8) Chen, M. H.; Lu, H.; Dong, J.; Miao, L.; Zhou, M. F. *J. Phys. Chem. A* **2002**, *106*, 11456. Chen, M. H.; Zeng, A. H.; Lu, H.; Zhou, M. F. *J. Phys. Chem. A* **2002**, *106*, 3077.

(9) Huang, Z. G.; Zeng, A. H.; Dong, J.; Zhou, M. F. *J. Phys. Chem. A* **2003**, *107*, 2329.

(10) Park, M.; Hauge, R. H.; Kafafi, Z. H.; Margrave, J. L. *J. Chem. Soc., Chem. Commun*. **1985**, 1570.

(11) Maier, G.; Reisenauer, H. P.; Egenolf, H. *Monatsh. Chem.* **1999**, *130*, 227.

(12) Khabashesku, V. N.; Kudin, K. N.; Margrave, J. L.; Fredin, L. *J. Organomet. Chem*. **2000**, *595*, 248.

(13) Lanzisera, D. V.; Andrews, L. *J. Phys. Chem. A* **1997**, *101*, 1482.

(14) Joly, H. A.; Howard, J. A.; Arteca, G. A. *Phys. Chem. Chem. Phys.* **2001**, *3*, 750.

(15) Ito, T.; Lunsford, J. H. *Nature* **1985**, *314*, 721. Lin, C. H.; Ito, H.; Wang, J.; Lunsford, J. H. *J. Am. Chem. Soc*. **1987**, *109*, 4808.

(16) Hu, C. W.; Yang, H. Q.; Wong, N. B.; Chen, Y. Q.; Gong, M. C.; Tian, A. M.; Li, C.; Li, W. K. *J. Phys. Chem. A* **2003**, *107*, 2316.

(17) Kauffman, J. W.; Hauge, R. H.; Margrave, J. L. *High Temp. Sci.* **1984**, *18*, 97.

(18) Chen, M. H.; Wang, X. F.; Zhang, L. N.; Yu, M.; Qin, Q. Z. *Chem. Phys*. **1999**, *242*, 81.

(19) Frisch, M. J.; Trucks, G. W.; Schlegel, H. B.; Scuseria, G. E.; Robb, M. A.; Cheeseman, J. R.; Zakrzewski, V. G.; Montgomery, J. A., Jr.; Stratmann, R. E.; Burant, J. C.; Dapprich, S.; Millam, J. M.; Daniels, A. D.; Kudin, K. N.; Strain, M. C.; Farkas, O.; Tomasi, J.; Barone, V.; Cossi, M.; Cammi, R.; Mennucci, B.; Pomelli, C.; Adamo, C.; Clifford, S.; Ochterski, J.; Petersson, G. A.; Ayala, P. Y.; Cui, Q.; Morokuma, K.; Malick, D. K.; Rabuck, A. D.; Raghavachari, K.; Foresman, J. B.; Cioslowski, J.; Ortiz, J. V.; Baboul, A. G.; Stefanov, B. B.; Liu, G.; Liashenko, A.; Piskorz, P.; Komaromi, I.; Gomperts, R.; Martin, R. L.; Fox, D. J.; Keith, T.; Al-Laham, M. A.; Peng, C. Y.; Nanayakkara, A.; Gonzalez, C.; Challacombe, M.; Gill, P. M. W.; Johnson, B.; Chen, W.; Wong, M. W.; Andres, J. L.; Gonzalez, C.; Head-Gordon, M.; Replogle, E. S.; Pople, J. A. *Gaussian 98*, Revision A.7; Gaussian, Inc.: Pittsburgh, PA, 1998.

(20) Becke, A. D. *J. Chem. Phys*. **1993**, *98*, 5648.

(21) Lee, C.; Yang, E.; Parr, R. G. *Phys. Rev. B* **1988**, *37*, 785.

(22) McLean, A. D.; Chandler, G. S. *J. Chem. Phys*. **1980**, *72*, 5639.

(23) Krishnan, R.; Binkley, J. S.; Seeger, R.; Pople, J. A. *J. Chem. Phys*.**1980**, *72*, 650.

(24) Head-Gordon, M.; Pople, J. A.; Frisch, M. *Chem. Phys. Lett*. **1988**, *153*, 503.

(25) Curtiss, L. A.; Raghavachari, K.; Redfern, P. C.; Pople, J. A. *J. Chem. Phys*. **1997**, *106*, 1063. Bauschlicher, C. W., Jr.; Ricca, A.; Partridge, H.; Langhoff, S. R. In *Recent Advances in Density Functional Theory*-;Chong, D. P., Ed.; World Scientific Publishing: Singapore, 1997; Part II. Bauschlicher, C. W., Jr.; Maitre, P. *J. Chem. Phys*. **1995**, *99*, 3444. Bytheway, I.; Wong, M. W. *Chem. Phys. Lett*. **1998**, *282*, 219.

(26) Miao, L.; Dong, J.; Yu, L.; Zhou, M. F. *J. Phys. Chem. A* **2003**, *107*, 1935.

(27) Lee, Y. K.; Manceron, L.; Papai, I. *J. Phys. Chem. A* **1997**, *101*, 9650.

(28) Bauschlicher, C. W., Jr.; Langhoff, S. R. *Spectrochim. Acta A* **1997**, *53*, 1205.

(29) Hudgins, D. M.; Allamandola, L. J. *J. Phys. Chem*. **1995**, *99*, 8978.

(30) *CRC handbook*; CRC Press: Boca Raton, FL, 1985.

(31) Andrews, L.; Chertihin, G. V.; Thompson, C. A.; Dillon, J.; Byrne, S.; Bauschlicher, C. W., Jr. *J. Phys. Chem*. **1996**, *100*, 10088.